

CrossMark
click for updatesCite this: *J. Mater. Chem. A*, 2016, 4, 6029

Mo₂C as a high capacity anode material: a first-principles study

Deniz Çakır,^{*a} Cem Sevik,^b Oğuz Gülseren^c and Francois M. Peeters^a

The adsorption and diffusion of Li, Na, K and Ca atoms on a Mo₂C monolayer are systematically investigated by using first principles methods. We found that the considered metal atoms are strongly bound to the Mo₂C monolayer. However, the adsorption energies of these alkali and earth alkali elements decrease as the coverage increases due to the enhanced repulsion between the metal ions. We predict a significant charge transfer from the ad-atoms to the Mo₂C monolayer, which indicates clearly the cationic state of the metal atoms. The metallic character of both pristine and doped Mo₂C ensures a good electronic conduction that is essential for an optimal anode material. Low migration energy barriers are predicted as small as 43 meV for Li, 19 meV for Na and 15 meV for K, which result in the very fast diffusion of these atoms on Mo₂C. For Mo₂C, we found a storage capacity larger than 400 mA h g⁻¹ by the inclusion of multilayer adsorption. Mo₂C expands slightly upon deposition of Li and Na even at high concentrations, which ensures the good cyclic stability of the atomic layer. The calculated average voltage of 0.68 V for Li and 0.30 V for Na ions makes Mo₂C attractive for low charging voltage applications.

Received 4th March 2016
Accepted 18th March 2016

DOI: 10.1039/c6ta01918h

www.rsc.org/MaterialsA

1 Introduction

Two-dimensional (2D) materials are expected to become key components for not only electronic devices (such as field effect transistors,¹ p–n junctions^{2,3} and so on) but also for energy storage applications including supercapacitors⁴ and batteries.⁵ Rechargeable batteries based on 2D materials with high energy storage density, high rate capacity and good cycling stability have attracted growing interest because of their great potential for use in portable electronic devices and electric vehicles. Therefore, searching for promising anode materials with enhanced gravimetric and volumetric energy densities is a key challenge for rechargeable ion batteries. In spite of its low capacity and weak binding energy of alkali atoms, graphite is extensively used as an anode material due to its low cost, high energy storage and cycling performance.^{6,7} Even though a single layer of graphite, called graphene, has been shown to exhibit much better electrochemical properties in lithium-ion battery applications,^{8–10} other 2D layered materials such as transition metal dichalcogenides,^{11,12} MXenes (with M = Ti, V, Nb, Mo and X = C, N)^{13–17} and black phosphorus^{18–20} have also been widely investigated because of their high energy storage density and high rate capacity.

Large area high quality 2D Mo₂C has recently been fabricated by using chemical vapour deposition (CVD).²¹ Due to its good electrical conductivity and its 2D structure, Mo₂C can serve as an anode material for metal-ion batteries. In this respect, we investigate adsorption and diffusion of alkali (Li, Na and K) and earth alkali (Ca) elements on a single layer of Mo₂C. Among the elements considered in this work, sodium is particularly important, because of its abundance and low cost.

The present paper is organized as follows. We first present our computational methodology in Section 2. Then, we address the structure and dynamical stability of the Mo₂C monolayer in Section 3. Our results for adsorption and diffusion of Li, Na, K and C on the monolayer Mo₂C are given in Section 4. We also discuss the effect of adatom concentration on the stability, capacity and voltage profile of Mo₂C based ion batteries in Section 5. Finally, we conclude with an overview of our main results in Section 6.

2 Computational method

We carry out first-principles calculations in the framework of density functional theory (DFT) as implemented in the Vienna ab-initio simulation package (VASP).^{22,23} The generalized gradient approximation (GGA) within the Perdew–Burke–Ernzerhof (PBE)²⁴ formalism is employed for the exchange–correlation potential. The projector augmented wave (PAW) method²⁵ is used to take into account the electron–ion interaction. A plane-wave basis set with an energy cutoff of 500 eV is used in the calculations. For geometry optimization the Brillouin-zone integration is performed using a regular Γ centered $21 \times 21 \times 1$

^aDepartment of Physics, University of Antwerp, Groenenborgerlaan 171, 2610 Antwerpen, Belgium. E-mail: dcakir79@gmail.com; francois.peeters@uantwerpen.be

^bDepartment of Mechanical Engineering, Faculty of Engineering, Anadolu University, Eskisehir, TR 26555, Turkey. E-mail: csevik@anadolu.edu.tr

^cDepartment of Physics, Bilkent University, Bilkent, Ankara 06800, Turkey. E-mail: gulseren@fen.bilkent.edu.tr

k -mesh for the unit cell of Mo_2C within the Monkhorst-Pack scheme.²⁶ The convergence criterion of the self-consistent field calculations is set to 10^{-5} eV for the total energy. To prevent spurious interaction between isolated monolayers, a vacuum spacing of at least 15 Å is introduced. By using the conjugate gradient method, atomic positions and lattice constants are optimized until the Hellmann–Feynman forces are less than 0.01 eV \AA^{-1} and pressure on the supercell is decreased to values less than 1 kbar.

Diffusion barriers for alkali and earth alkali atoms are calculated using the climbing-image nudge elastic (CI-NEB) method as implemented in the VASP transition state tools.^{27,28} CI-NEB is an efficient method in determining the minimum energy diffusion path between two given positions. For a single atom diffusion on a 4×4 Mo_2C monolayer, we used 12 images, including initial and final positions, for CI-NEB calculations. The atomic positions and energy of the images are then relaxed until the largest norm of the force orthogonal to the path is smaller than 0.01 eV \AA^{-1} . The amount of charge transfer between alkali/earth alkali atom and Mo_2C is determined by using the Bader charge analysis.^{29–31}

3 Structure and stability of Mo_2C

The structure of Mo_2C can be viewed as bilayer Mo-atomic layers intercalated by a C layer forming an edge-shared Mo_6C octahedral structure as shown in Fig. 1. First, we predict the equilibrium lattice properties corresponding to this structure. The lattice constant, a_0 , and Mo–C interatomic distance are determined to be 2.99 Å and 2.08 Å, respectively. The dynamical stability was investigated from a calculation of the vibrational spectrum of the structure by the help of accurate phonon calculations based on density functional perturbation theory.³² The results clearly prove that free standing Mo_2C is free of

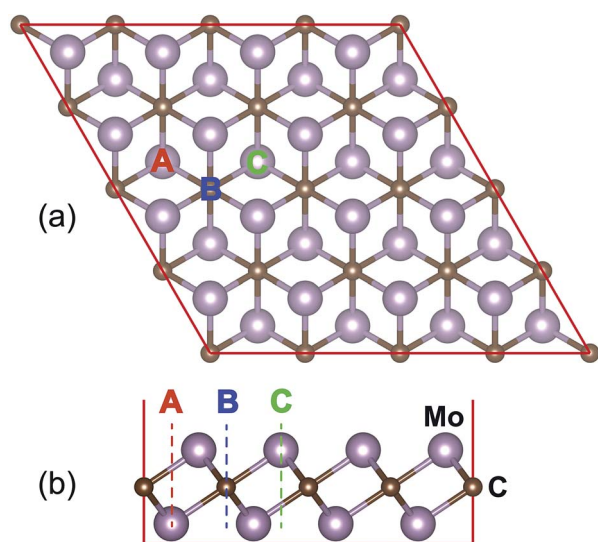


Fig. 1 Top and side view of the optimized structure of the Mo_2C monolayer. (A–C) represent the possible adsorption sites for metal atoms.

imaginary vibrational frequencies, which otherwise would be a sign of instability, see Fig. 2. The irreducible representation of the vibrational modes at the Γ -point is as follows,

$$\Gamma = 2E_u \oplus A_{2u} \oplus 2E_g \oplus A_{1g} \oplus 2E_u \oplus A_{2u}. \quad (1)$$

The first three modes, (*i.e.* $2E_u$ and A_{2u}), are acoustic and inherently have zero frequencies at the Γ point. The other six modes include three Raman- (*i.e.* $2E_g$ and A_{1g}) and three infrared (IR)-active (*i.e.* $2E_u$ and A_{2u}) optical modes with frequencies calculated to be 157, 228, 642, and 657 cm^{-1} , respectively. Here, a significant gap between the Raman- and IR-active modes of about 400 cm^{-1} is quite striking.

4 Adatom adsorption and diffusion

Next, we examine the performance of this material as an anode material in battery applications. A relatively strong binding energy with metal atoms is a necessary prerequisite in order to be a promising anode material. Therefore, we investigate the binding energy, E_{bind} , of a single metal atom on a Mo_2C monolayer using the following equation,

$$E_{\text{bind}} = E_{\text{Mo}_2\text{C}M_x} - E_{\text{Mo}_2\text{C}} - xE_M \quad (2)$$

where $E_{\text{Mo}_2\text{C}M_x}$, $E_{\text{Mo}_2\text{C}}$ and E_M are the total energies of metal-adsorbed Mo_2C , of the pristine Mo_2C monolayer and of a metal atom in its most stable bulk structure, respectively. Here, we use a body centered cubic bulk structure for Li, Na and K and a face centered cubic bulk structure for Ca. In accordance with this definition, E_{bind} becomes more negative for a more energetically favorable interaction between the metal atom and Mo_2C . As depicted in Fig. 1(a), three possible adsorption sites, namely A, B and C, are considered. The site A is at the center of a hexagon composed of carbon atoms, the site B is directly above a carbon atom and C site is directly above a Mo atom. In the calculations, a 4×4 supercell structure is used in order to avoid the

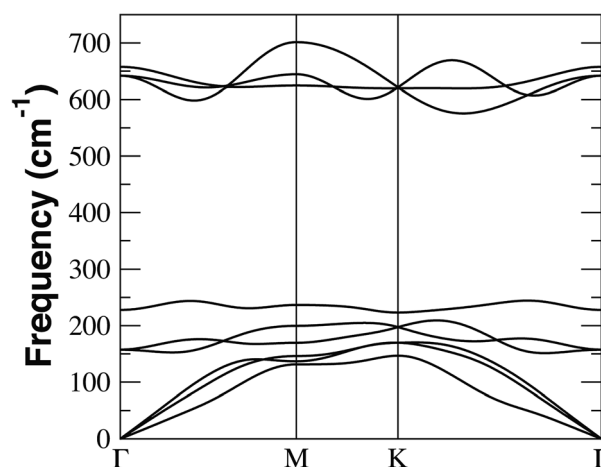


Fig. 2 Calculated phonon dispersion along the high symmetry directions for the pristine Mo_2C monolayer.

interaction between the metal atoms that are bound to the surface. The calculated binding energies reveal that adsorption on site C is energetically less favorable and site A is slightly more stable than site B for all metal atoms addressed in our study, see Table 1. Moreover, the calculated E_{bind} values at site A are -0.97 eV for Li, -1.18 eV for Na, -1.54 eV for K and -1.45 eV for Ca, which clearly indicates the stability of the Mo_2C -metal complex over segregated phases at 0 K. Therefore, from now on, we restrict ourselves in the following discussions to the adsorption on site A.

In order to gain further insight into the adsorption of the metal atoms, we also calculate the vertical distance between the metal atom and the topmost surface Mo layer, *i.e.* the adatom height (h) that measures the interaction strength of different metal atoms with Mo_2C . As is shown in Table 1, h increases as the mass of the metal atom increases in each metal group. For instance, the calculated h value is 2.37 Å for Li, and 3.20 Å for K. Fig. 3 depicts the variation of the total energy of the Li- Mo_2C system as a function of h . The change in total energy for the h values larger than 8 Å is negligible due to the quite weak interaction between the Li atom and the Mo_2C layer for these h values. On the other hand, a remarkable total energy difference, ~ 2.5 eV, between the Li- Mo_2C systems with $h = 2.35$ Å (equilibrium h value of the Li atom) and $h = 12$ Å clearly elucidates the strong interaction between the Li atom and the Mo_2C layer. As is evident from Fig. 3, the interaction between the Li ion and the Mo_2C monolayer is mainly dominated by the Coulomb interaction, and thus the van der Waals contribution can be neglected. Furthermore, Fig. 3 shows that the metal ion does not encounter any energy barrier as it approaches the Mo_2C layer.

Mo_2C exhibits metallic behavior with a good electrical conductivity which is a vital factor to decide about the electrochemical performance of an electrode and ensures good cycling stability. On account of this, we investigate the electronic properties of Mo_2C with and without the adsorbed metal atom. Fig. 4 depicts the total and projected density of states. Since the metal atom concentration is low in these electronic structure calculations ($1/16$ metal atom per formula unit), the total DOS of the doped Mo_2C is similar to that of pristine Mo_2C . As is seen from Fig. 4, the Mo_2C monolayer remains metallic upon adsorption of metal atoms. We observe a significant overlap within $[-2, 0]$ eV between the Mo d orbital and the metal s orbital, indicating a s-d hybridization. This further proves the strong binding of the metal atoms on Mo_2C .

Table 1 also summarizes the amount of charge transfer from the adsorbed metal atom to Mo_2C . The Bader charge analysis

Table 1 Binding energies for adsorption at sites (see Fig. 1b) A, B and C in eV, the adatom height from the Mo_2C monolayer for site A (in Å) and the Bader charge on the metal atoms adsorbed at site A

	$E_{\text{bind}}^{\text{A}}$	$E_{\text{bind}}^{\text{B}}$	$E_{\text{bind}}^{\text{C}}$	h^{A}	Q_{M}^{A}
Li	-0.97	-0.94	-0.83	2.37	0.989
Na	-1.18	-1.17	-1.10	2.73	0.987
K	-1.54	-1.53	-1.52	3.20	0.802
Ca	-1.45	-1.35	-1.30	2.53	1.223

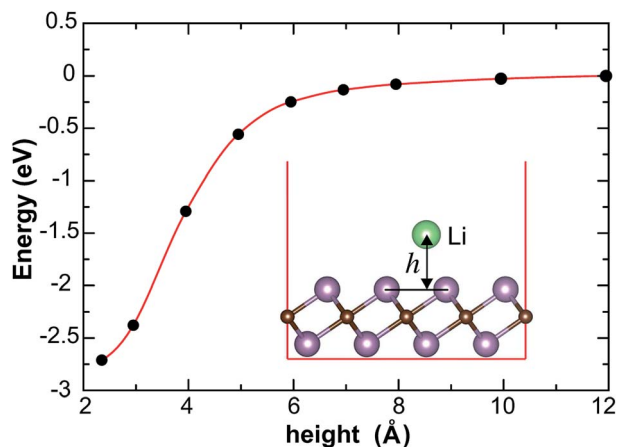


Fig. 3 Change of total energy of the Li- Mo_2C system as a function of vertical distance between the Li atom and the Mo_2C monolayer.

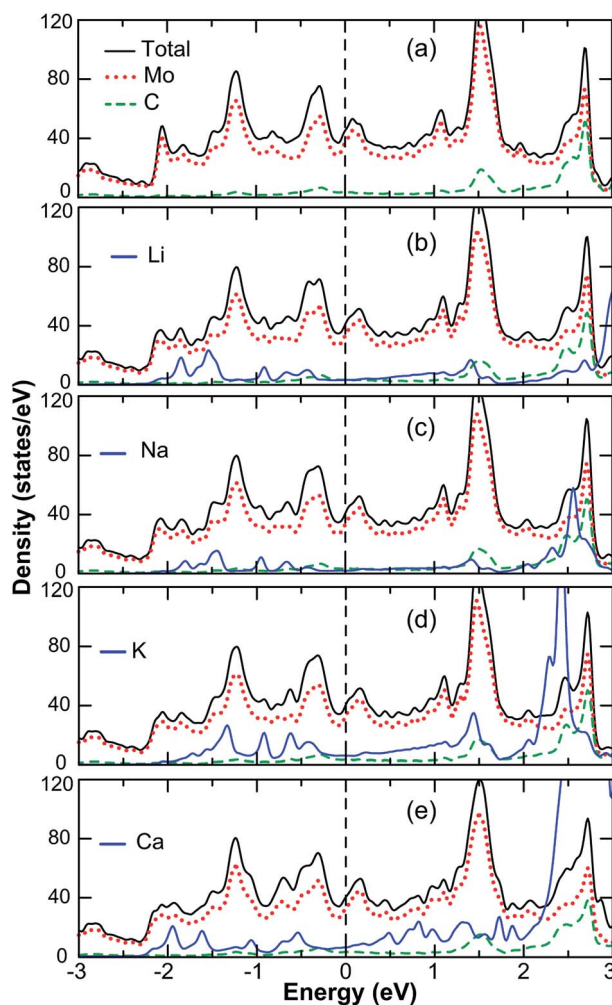


Fig. 4 Total and partial DOS for (a) pristine, (b) Li, (c) Na, (d) K and (e) Ca doped Mo_2C . The PDOS of the metal ions (multiplied with 100 for Li, Na and K and 25 for Ca) and C (multiplied with 4) atoms is enlarged in order to make them visible. The Fermi level is set to zero energy.

reveals that Li and Na atoms donate almost their *s* electron to Mo₂C. The Ca atom donates more than one electron to Mo₂C. The Bader charge values suggest that metal ions are in the cationic state upon deposition on the Mo₂C monolayer.

A low diffusion barrier and high mobility are desired properties for a promising electrode material. In particular, the mobility of a metal atom on an electrode material is a key factor determining the rate performance at which a battery can be charged and discharged. Therefore we investigate the diffusion barriers for Li, Na, K and Ca along two different possible migration paths, namely path 1 and path 2, that are selected between two adjacent lowest energy adsorption sites on the Mo₂C layer, see the inset of the lower left panel of Fig. 5. Fig. 5 shows the diffusion barriers and optimized pathways for all considered metal atoms. The calculated diffusion barrier for path 1 (path 2) is 43 (93) meV for Li, 19 (49) meV for Na, 15 meV for K and 110 (130) meV for Ca. The small diffusion barriers predicted for Na and K can be partly due to their larger *h* values (as compared to Li and Ca) and the surface-confined electron layer that effectively smooths the potential on the surface. For the case of Li and Na diffusion along path 1, there are two peaks with almost the same barrier values and there is a local minimum between these two saddle points, corresponding to the adsorption of the Li/Na atom at a metastable site (*i.e.* site B). Due to its larger atomic size, path 1 and path 2 have similar migration profiles for the Ca ion. We find that the K ion has the smallest migration barrier amongst studied metal atoms. Compared to the Li diffusion barrier of 0.25 eV on MoS₂,¹¹ 0.22 eV on VS₂,¹¹ 0.068 eV on Ti₂C₃,¹⁵ 0.33 eV on graphene,³³ and 0.084 eV on black phosphorus,¹⁹ Mo₂C facilitates a faster transport and higher charge/discharge rate not only for Li but also for other alkali and earth alkali elements. Moreover, the calculated diffusion barriers are smaller than the energy barrier for Li diffusion in commercially used anode materials based on TiO₂ with a barrier of 0.35–0.65 eV (ref. 34–36) and high-capacity bulk silicon anode materials with a diffusion barrier around 0.57 eV. Similar to other 2D materials, due to their large surface area, Mo₂C based electrodes are expected to significantly increase the storage capacity of batteries.

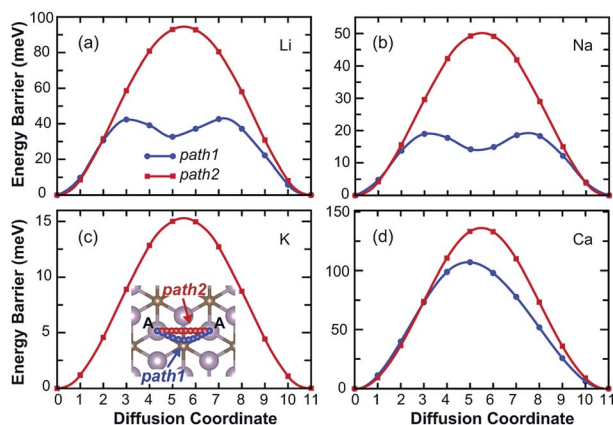


Fig. 5 Diffusion barrier profiles of (a) Li, (b) Na, (c) K and (d) Ca. The inset of (c) depicts the two possible optimized migration pathways between two nearest A sites.

The diffusion coefficient, *D*, for such a problem can be estimated *via* the Arrhenius equation,

$$D \approx \exp\left(\frac{-E_a}{k_B T}\right), \quad (3)$$

where E_a is the activation energy for diffusion, k_B is the Boltzmann constant, and T is the temperature. Therefore, we can roughly estimate the room temperature mobility of metal ions on the Mo₂C surface by using this simple equation. We find that the room temperature Li (Na) mobility on Mo₂C is approximately 3×10^3 (7.6×10^3) and 6.6×10^4 (1.7×10^5) times faster than that on MoS₂ and graphene, respectively.

Until now, we only consider single atom adsorption and diffusion on the Mo₂C monolayer. To get a more complete picture, we also investigate Li and Na intercalation into bulk Mo₂C and their diffusion within the material. We calculate the diffusion path and the energy barrier for a vacancy in a $3 \times 3 \times 1$ supercell, where all Li/Na atoms only occupy site A as seen in Fig. 6(a). We should mention that bulk Mo₂C is not able to store K/Ca as much as Li/Na. Regarding the storage capacity, K and Ca are not appropriate elements for Mo₂C based battery applications. Therefore, we only focus on Li and Na. Our results indicate that, for a dilute vacancy concentration, the vacancy hops between two neighboring sites (*i.e.* site A) and the corresponding energy barriers are 0.27 eV for Li and 0.06 eV for Na, see Fig. 6(b). Consequently, a high-rate capacity is expected for Mo₂C-based alkali batteries even for bulk Mo₂C. Note that the lowest energy diffusion barrier profile of a Li/Na ion inside fully loaded bulk Mo₂C is found to be different from that of an isolated Li/Na ion on the 4×4 supercell structure of Mo₂C. For the former case, the repulsive interaction originating from the neighboring Li/Na ions significantly modifies the diffusion profile. Therefore, for large concentrations, the diffusion barrier profile depicted in Fig. 6(b) should be expected.

5 Effect of adsorbent concentration and theoretical voltage profile

The open-circuit-voltage value is a measure of the performance of a battery. Roughly, it can be approximated by calculating the average voltage over a range of metal ion concentrations. The

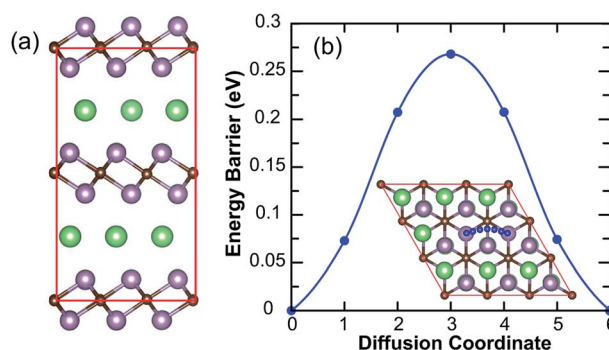


Fig. 6 (a) Optimized structure of the Mo₂C–Li complex and (b) diffusion barrier and path (see blue dots in the inset) of a Li ion.

charge/discharge processes of Mo_2C follow the common half-cell reaction *vs.* M/M^+ :



Considering the above reaction, the average voltage of Mo_2CM_x in the concentration range of $x_1 \leq x \leq x_2$ is given by,^{37–39}

$$V \approx \frac{E_{\text{Mo}_2\text{CM}_{x_1}} - E_{\text{Mo}_2\text{CM}_{x_2}} + (x_2 - x_1)E_{\text{M}}}{(x_2 - x_1)e} \quad (5)$$

where $E_{\text{Mo}_2\text{CM}_{x_1}}$, $E_{\text{Mo}_2\text{CM}_{x_2}}$ and E_{M} are the total energy of $\text{Mo}_2\text{CM}_{x_1}$, $\text{Mo}_2\text{CM}_{x_2}$, and metallic M, respectively. In fact, for the calculation of the average voltage, Gibbs free energy ($G(x) = \Delta E + P\Delta V - T\Delta S$) should be considered. However, $P\Delta V$ is only on the order of 10^{-5} eV and the entropy term ($T\Delta S$) is around 25 meV at room temperature, and hence the first term (*i.e.* internal energy change) is sufficient to estimate the average voltage.³⁷

Before calculating V , we first study the effect of the metal ion concentration on E_{bind} . We place the metal atoms on site A. Fig. 7(a) shows the variation of E_{bind} as a function of concentration of the metal ions (*i.e.* x) adsorbed on one side of Mo_2C . Here, the concentration, x , corresponds to the number of the adsorbed atoms per formula unit of Mo_2C . The first clear observation is that E_{bind} decreases gradually with the increase of concentration due to the enhanced repulsive interaction

between the metal ions and the reduced interaction between the Mo_2C host and metal ions. The latter is correlated with the reduction of charge transfer from the metal atom to Mo_2C at high concentrations. Since K and Ca ions have larger ionic radius as compared to Li and Na, an increase in concentration results in a larger enhancement of the repulsive Coulomb interaction that significantly reduces the binding energy. After a critical concentration, this enhanced repulsive interaction makes $\text{Mo}_2\text{C-K}/\text{Mo}_2\text{C-Ca}$ systems energetically less stable with respect to the $\text{Mo}_2\text{C-Li}/\text{Mo}_2\text{C-Na}$ systems, see Fig. 7(a). E_{bind} is always negative for Li and Na, suggesting that the Mo_2CM complex is stable for these alkali elements, and thus we can safely disregard the phase separation problem at high concentrations. However, E_{bind} becomes positive for K and Ca before x reaches 1. These results demonstrate that Mo_2C can be utilized as an anode material for high capacity Li/Na ion batteries. In real battery applications, ion adsorption on both sides of Mo_2C should be expected. Fig. 7(b) shows the results for double-side adsorption. Except Li, double-side adsorption is more stable than single side adsorption for high metal ion concentrations. This is possibly ascribed to the reduction in repulsive interaction between the metal ions. Due to its smallest ionic radius, Li shows little sensitivity to concentration and its binding energy for any concentration remains unchanged upon introducing double side adsorption. In spite of their larger sizes, E_{bind} of K and Ca is also negative in double side adsorption for large x values.

Assuming double side adsorption, Mo_2CM_2 represents the highest metal ion storage capacity for the Mo_2C monolayer. A theoretical capacity of 263 mA h g^{-1} is obtained for Li and Na. Compared to the MoS_2 monolayer with a capacity of 335 mA h g^{-1} (ref. 11) and graphite with a capacity of 372 mA h g^{-1} ,⁴⁰ the Mo_2C monolayer provides a lower power density. Although Mo_2C generally is heavier than most of the 2D materials in terms of atomic weight, its storage capacity may be improved by the help of multilayer adsorption. In a recent study, it was experimentally shown that Nb_2C based MXenes have higher reversible Li capacities as compared to the Ti-containing ones whereas the former material class is significantly heavier than the latter.¹⁶ To test the feasibility of multilayer adsorption, we calculate the binding energy for a bilayer (trilayer) Li adsorption on both sides of Mo_2C . E_{bind} , calculated *via* eqn (2), is found to be -0.31 (-0.21) eV/Li for bilayer (trilayer). These results suggest that at least two more extra Li layers may be formed before a bulk-like arrangement of Li atoms becomes more favorable. In order to accommodate multilayer adsorption in bulk Mo_2C , a much larger spacing is needed between Mo_2C layers. Therefore, we believe that multilayer adsorption is expected to be limited to 2–3 layers of Li per side. For Mo_2CLi_4 (Mo_2CLi_6), the storage capacity becomes 526 (789) mA h g^{-1} which is sufficiently large for practical applications.

Another important point is how the stability of Mo_2C is affected as metal ion coverage increases. We find that an increase in the number of metal atoms adsorbed on the Mo_2C monolayer slightly enlarges the Mo–C interatomic bond lengths (at most 0.025 \AA for Li, Na and K and at most 0.05 \AA for Ca). In addition, the in-plane lattice constant of Mo_2C expands at most

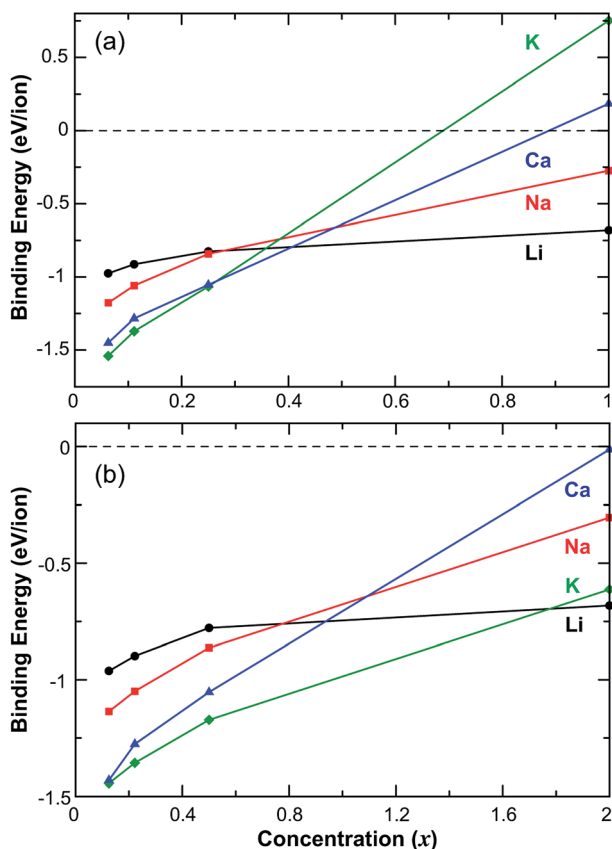


Fig. 7 Binding energy as a function of metal atom concentration (x): (a) single side and (b) double side adsorption.

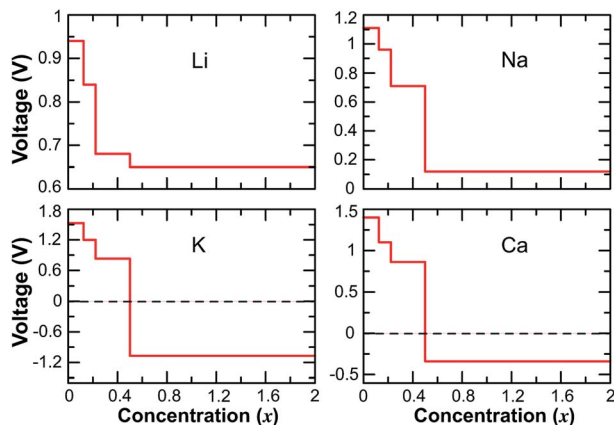


Fig. 8 Calculated voltage profile as a function of concentration for double side adsorption.

2% upon double side adsorption of Li and Na for $x = 2$. Therefore, we can expect that there will be no bond breaking for Mo_2C -based Li and Na-ion batteries in contrast to the case of black phosphorus,^{19,41} which ensures a good cycling stability. The lattice expansion is found to be much larger for K and Ca due to their larger ionic radius.

Finally, we calculate the average voltage (V) via eqn (5). The negative value of V for $x \geq 0.5$ V in Fig. 8 implies that $\text{Mo}_2\text{CK}_{0.5}/\text{Mo}_2\text{CCa}_{0.5}$ cannot accept more K or Ca to form $\text{Mo}_2\text{CK}_2/\text{Mo}_2\text{CCa}_2$ even though the double side binding energy of K/Ca in $\text{Mo}_2\text{CK}_2/\text{Mo}_2\text{CCa}_2$ is negative. Therefore, no more adatoms can be adsorbed by $\text{Mo}_2\text{CK}_{0.5}/\text{Mo}_2\text{CCa}_{0.5}$. Here $x = 0.5$ corresponds to the maximum achievable x for K and Ca. Therefore, we can expect the formation of metallic K/Ca for concentrations larger than 0.5, which is detrimental for battery applications. However, for $\text{Mo}_2\text{CLi}_x/\text{Mo}_2\text{CNa}_x$, x can be as high as 2. As we increase the Li (Na) concentration from $x = 0.5$ to $x = 2$, the open-circuit voltage decreases from 0.68 (0.71) V to 0.65 (0.12) V. The voltage averaged over $0 \leq x \leq 2$ is 0.68 V for Li and 0.30 V for Na, which is between those of the commercial anode materials, such as ~ 0.2 V for graphite⁴² and 1.5–1.8 V for TiO_2 .⁴³ The potential range of [0.1, 1] V is highly desired for an anode material. Therefore, Mo_2C -Li and Mo_2C -Na systems can be utilized for low voltage battery applications.

6 Conclusion

The calculated strong binding energies and small diffusion barriers indicate that Mo_2C is an appealing anode material. Mo_2C is intrinsically stable and is metallic, which is essential for battery applications. Upon adsorption, adatoms donate a significant amount of charge to Mo_2C and exist in the cationic state. In spite of their large binding energies, adatoms, especially Li, Na and K, are very mobile on Mo_2C with diffusion barriers of 43 meV for Li, 19 meV for Na and 15 meV for K. Moreover, we find that the achievable maximum stable concentration (*i.e.* x) for the $\text{Mo}_2\text{CLi}_x/\text{Mo}_2\text{CNa}_x$ and $\text{Mo}_2\text{CK}_x/\text{Mo}_2\text{CCa}_x$ is 2 and 0.5, respectively. The moderate storage capacity can significantly be improved by multilayer adsorption.

The calculated average voltage of adatom intercalation is 0.68 V for Li and 0.30 V for Na, which is suitable for low charging voltage applications. Its good electrical conductivity, fast ion diffusion, good average open-circuit voltage and theoretical capacity suggest that the Mo_2C monolayer can be utilized as a promising anode material for Li and Na ion batteries with high power density and fast charge/discharge rates. Compared to commercially available ion batteries, Mo_2C based Li and Na ion batteries offer much larger energy storage capacities and faster charge/discharge rates.

Acknowledgements

This work was supported by the Flemish Science Foundation (FWO-VI) and the Methusalem foundation of the Flemish government. Computational resources were provided by TUBITAK ULAKBIM, High Performance and Grid Computing Center (TR-Grid e-Infrastructure), and HPC infrastructure of the University of Antwerp (CalcUA) a division of the Flemish Supercomputer Center (VSC), which is funded by the Hercules foundation. C. S. acknowledges the support from Turkish Academy of Sciences (TUBA-GEBIP). C. S. acknowledges the support from Anadolu University (Grant No. 1407F335). We acknowledge the support from TUBITAK, The Scientific and Technological Research Council of Turkey (Grant No. 115F024).

References

- 1 B. Radisavljevic, A. Radenovic, J. Brivio, V. Giacometti and A. Kis, *Nat. Nanotechnol.*, 2011, **6**, 147.
- 2 D. Çakır, D. Kecik, H. Sahin, E. Durgun and F. M. Peeters, *Phys. Chem. Chem. Phys.*, 2015, **17**, 13013–13020.
- 3 M.-Y. Li, Y. Shi, C.-C. Cheng, L.-S. Lu, Y.-C. Lin, H.-L. Tang, M.-L. Tsai, C.-W. Chu, K.-H. Wei, J.-H. He, W.-H. Chang, K. Suenaga and L.-J. Li, *Science*, 2015, **349**, 524–528.
- 4 M. Acerce, D. Voiry and M. Chhowalla, *Nat. Nanotechnol.*, 2015, **10**, 313–318.
- 5 G. Zhou, F. Li and H.-M. Cheng, *Energy Environ. Sci.*, 2014, **7**, 1307–1338.
- 6 A. Doron, Z. Ella, C. Yaron and T. Hanan, *Solid State Ionics*, 2002, **148**, 405–416.
- 7 M. Yoshio, H. Wang and K. Fukuda, *Angew. Chem., Int. Ed.*, 2003, **42**, 4203–4206.
- 8 E. Yoo, J. Kim, E. Hosono, H. Shen Zhou, T. Kudo and I. Honma, *Nano Lett.*, 2008, **8**, 2277–2282.
- 9 K. S. Novoselov, A. K. Geim, S. V. Morozov, D. Jiang, Y. Zhang, S. V. Dubonos, I. V. Grigorieva and A. A. Firsov, *Science*, 2004, **306**, 666–669.
- 10 K. S. Novoselov, A. K. Geim, S. V. Morozov, D. Jiang, M. I. Katsnelson, I. V. Grigorieva, S. V. Dubonos and A. A. Firsov, *Nature*, 2005, **438**, 197–200.
- 11 Y. Jing, Z. Zhou, C. R. Cabrera and Z. Chen, *J. Phys. Chem. C*, 2013, **117**, 25409–25413.
- 12 E. Yang, H. Ji and Y. Jung, *J. Phys. Chem. C*, 2015, **119**, 26374–26380.
- 13 J. Hu, B. Xu, S. A. Yang, S. Guan, C. Ouyang and Y. Yao, *ACS Appl. Mater. Interfaces*, 2015, **7**, 24016–24022.

- 14 J. Zhu, A. Choneos and U. Schwingenschlöggl, *Phys. Status Solidi RRL*, 2015, **9**, 726–729.
- 15 D. Er, J. Li, M. Naguib, Y. Gogotsi and V. B. Shenoy, *ACS Appl. Mater. Interfaces*, 2014, **6**, 11173–11179.
- 16 C. Eames and M. S. Islam, *J. Am. Chem. Soc.*, 2014, **136**, 16270–16276.
- 17 M. Naguib, J. Halim, J. Lu, K. M. Cook, L. Hultman, Y. Gogotsi and M. W. Barsoum, *J. Am. Chem. Soc.*, 2013, **135**, 15966–15969.
- 18 J. Sun, H.-W. Lee, M. Pasta, H. Yuan, G. Zheng, Y. Sun, Y. Li and Y. Cui, *Nat. Nanotechnol.*, 2015, **10**, 980–985.
- 19 W. Li, Y. Yang, G. Zhang and Y.-W. Zhang, *Nano Lett.*, 2015, **15**, 1691–1697.
- 20 V. V. Kulish, O. I. Malyi, C. Persson and P. Wu, *Phys. Chem. Chem. Phys.*, 2015, **17**, 13921–13928.
- 21 C. Xu, L. Wang, Z. Liu, L. Chen, J. Guo, N. Kang, X.-L. Ma, H.-M. Cheng and W. Ren, *Nat. Mater.*, 2015, **14**, 1135–1141.
- 22 G. Kresse and J. Furthmüller, *Comput. Mater. Sci.*, 1996, **6**, 15.
- 23 G. Kresse and J. Furthmüller, *Phys. Rev. B: Condens. Matter Mater. Phys.*, 1996, **54**, 11169–11186.
- 24 J. P. Perdew, K. Burke and M. Ernzerhof, *Phys. Rev. Lett.*, 1996, **77**, 3865–3868.
- 25 P. E. Blöchl, *Phys. Rev. B: Condens. Matter Mater. Phys.*, 1994, **50**, 17953–17979.
- 26 H. J. Monkhorst and J. D. Pack, *Phys. Rev. B: Condens. Matter Mater. Phys.*, 1976, **13**, 5188–5192.
- 27 G. Henkelman, B. P. Uberuaga and H. Jansson, *J. Chem. Phys.*, 2000, **113**, 9901–9904.
- 28 G. Henkelman and H. Jansson, *J. Chem. Phys.*, 2000, **113**, 9978–9985.
- 29 W. Tang, E. Sanville and G. Henkelman, *J. Phys.: Condens. Matter*, 2009, **21**, 084204.
- 30 E. Sanville, S. D. Kenny, R. Smith and G. Henkelman, *J. Comput. Chem.*, 2007, **28**, 899.
- 31 G. Henkelman, A. Arnaldsson and H. Jónsson, *Comput. Mater. Sci.*, 2006, **36**, 254.
- 32 S. Baroni, S. de Gironcoli, A. Dal Corso and P. Giannozzi, *Rev. Mod. Phys.*, 2001, **73**, 515–562.
- 33 C. Uthaisar and V. Barone, *Nano Lett.*, 2010, **10**, 2838–2842.
- 34 S. Lunell, A. Stashans, L. Ojamae, H. Lindstrom and A. Hagfeldt, *J. Am. Chem. Soc.*, 1997, **119**, 7374–7380.
- 35 H. Lindström, S. Sadegren, A. Solbrand, H. Rensmo, J. Hjelm, A. Hagfeldt and S.-E. Lindquist, *J. Phys. Chem. B*, 1997, **101**, 7710–7716.
- 36 C. L. Olson, J. Nelson and M. S. Islam, *J. Phys. Chem. B*, 2006, **110**, 9995–10001.
- 37 M. K. Aydinol, A. F. Kohan, G. Ceder, K. Cho and J. Joannopoulos, *Phys. Rev. B: Condens. Matter Mater. Phys.*, 1997, **56**, 1354–1365.
- 38 R. E. Doe, K. A. Persson, Y. S. Meng and G. Ceder, *Chem. Mater.*, 2008, **20**, 5274–5283.
- 39 F. Zhou, M. Cococcioni, C. A. Marianetti, D. Morgan and G. Ceder, *Phys. Rev. B: Condens. Matter Mater. Phys.*, 2004, **70**, 235121.
- 40 Y. Liu, V. I. Artyukhov, M. Liu, A. R. Harutyunyan and B. I. Yakobson, *J. Phys. Chem. Lett.*, 2013, **4**, 1737–1742.
- 41 J. Sun, G. Zheng, H.-W. Lee, N. Liu, H. Wang, H. Yao, W. Yang and Y. Cui, *Nano Lett.*, 2014, **14**, 4573–4580.
- 42 K. Persson, Y. Hinuma, Y. S. Meng, A. Van der Ven and G. Ceder, *Phys. Rev. B: Condens. Matter Mater. Phys.*, 2010, **82**, 125416.
- 43 M. V. Koudriachova, N. M. Harrison and S. W. de Leeuw, *Solid State Ionics*, 2002, **152–153**, 189–194.